Multirotor wind turbine - drag

Marius Hansen

Camilla Leikvoll

Magnus Vikse

Bachelor's thesis in Energy technology

Bergen, Norway 2021

Høgskulen
på Vestlandet

Multirotor wind turbine - drag

Marius Hansen

Camilla Leikvoll

Magnus Vikse

Department of Mechanical- and Marine Engineering

Western Norway University of Applied Sciences

NO-5063 Bergen, Norway

IMM 2021-M68

III

Høgskulen på Vestlandet

Fakultet for Ingeniør- og Naturvitenskap

Institutt for maskin- og marinfag

Inndalsveien 28

NO-5063 Bergen, Norge

Norsk tittel: Multirotor vind turbin - drag

Author(s), student number: Marius Hansen, h580847

Camilla Leikvoll, h580852

Magnus Vikse, h181284

Study program: Energy technology

Date: May 2021

Report number: IMM 2021-M68

Supervisor at HHVL: Jan Michael Simon Bartl

Assigned by: HVL

Contact person: Jan Michael Simon Bartl

Antall filer levert digitalt: 5/5

Preface

This thesis is written as a part of the bachelor program of Energy technology, for Western Norway University of applied science, at the department of Mechanical and Marine Engineering, campus Bergen.

We would like in association with this thesis to thank lab engineers Harald Moen and Frode Wessel Jansen for helping us with lab setup and calibration of loadcell. A special thanks to Jan Michael Simon Bartl our supervisor for being available at all times of the day through the whole semester, and for guidance in MatLab.

We are grateful for this opportunity with so many helpful people and a very exciting subject. An extra thanks to family and loved ones for support through this thesis.

Abstract

The world is in a transitional phase, moving from fossil energy sources to renewable energy, and wind energy is a vital part of this transition. In this process there is a development of more efficient wind turbines, which include new technologies like a multirotor wind turbine (MR). This type of wind turbine consists of multiple rotors connected to a single support structure. With a multirotor setup an effect called blockage effect occurs and it is present when multiple rotors are placed close to each other. Questions linked to multirotors is if the cost or weight will be improved in comparison with the singlerotor. This can lead to simpler transport and installations, which may impact the future development of wind energy.

In this thesis there has been implemented drag force measurement on a multirotor with seven turbines (MR7), four turbines (MR4), and two single-rotors (SR). With the measurements it is possible to compare the drag forces on several MR and SR-systems. In this small-scale experiment, the rotors are represented by one or multiple actuator discs. The tests are performed in a towing tank in the Marin Lab in Western Norway University of Applied Science, and the MR-system is tested with different velocities and with several distances between the disc to assess how the total drag is affected by the inter-rotor diameter. In this thesis it will be investigated if there is an optimal distance between the discs which gives the greatest drag value.

Sammendrag

Verden står fremfor et grønt skifte i energi-produksjonen og vindenergi står sentralt i denne utviklingen. Denne prosessen innebærer at det utvikles nye og mer effektive vindturbiner, og en multirotor vindturbin (MR) er med på denne utviklingen. Denne typen turbin består av flere rotorer satt sammen ved en støttestruktur for å holde de på plass. Med en multirotor vindturbin oppstår det en effekt som kalles for blokasje effekten, og denne inntreffer når flere rotorer står samlet. Spørsmål knyttet til en multirotor er om det vil gi fordeler på kostnader og vekt i forhold til en singelrotor. Dette kan føre til enklere frakt og installering, som er med på å gjøre det enklere å bygge ut mer i fremtiden.

I denne oppgaven er det gjort eksperimenter på en multirotor med syv turbiner (MR7), fire turbiner (MR4) og to ulike singelrotorer (SR). Målingene beregner drag krefter, som er motstanden som MR-systemet lager. Siden dette er et små-skala eksperiment er rotorene erstattet med aktuator disker. Testen gjennomføres i en vanntank på marinlaben på Høgskulen på Vestlandet, og MR-systemet testes på ulike hastigheter og distanser mellom diskene for å se hvordan dragkreftene-øker. Det skal i denne oppgaven undersøkes om det finnes en optimal distanse mellom diskene som gir den største drag verdien.

Table of contents

Nomenclature

ρ = Density [kg/m^3]

F_d = Drag force [N]

C_d = Drag coefficient

MR [X] = Multirotor [Number of discs]

SR = Singlerotor

SMR = Structure of multirotor

d = Diameter

C$_p$ = Power Coefficient

A = Area

CAD = Computer-Aided Design

Re = Reynolds number

μ = Viscosity of the fluid

l = Length

1. Introduction

Global warming and climate change forces the world to think in new courses for a sustainable energy production. The Paris Agreement developed by UN contains a goal to limit average global temperatures increasing to more than 2° C, preferably to 1.5° C, compared to pre-industrial levels [1]. This requires new technology, knowledge, and creative minds to make a transition from fossil fuels to renewable energy sources. According to the BP's statistics from 2019, 84,3% of the world energy production comes from fossil fuels, 11,4% from renewable, and the rest from other sources, primarily nuclear energy [2]. If the Paris agreement is to be fulfilled, the usage of fossil fuels needs to be decreased. Over the last couple of years, the public and companies are taking a more active part in the 'green change'. This leads to people being more conscious about global warming, and the necessary actions to counteract it. One example of this is Equinor, the largest company in Norway, which has primarily been an oil and gas company since it was established in 1972. In 2018 they had a name change from Statoil to Equinor, to mark the change, where they will be focusing more on renewable energy sources. Today they are part of wind and solar projects around the world, such as the Hywind Scotland wind park and the Apodi solar plant in Brazil, marking a change in the wind [3].

Wind power is on the rise worldwide, and one of the fastest-growing renewable energy technologies. The latest data from IRENA an intergovernmental organisation shows that 16% of renewable comes from wind energy, both onshore and offshore [4]. The growth of wind energy has increased from 7.5 GW in 1997 to 564 GW by 2018, giving a growth of almost 7500%, or in other words, 75 times larger. [4] The growth is increasing due to cost reduction in production of wind turbines, and the key parameters to this reduction are improvements in wind turbine technology, by enlarging the rotor diameter and hub height to access more power from the wind [5]. Today the larges wind turbine operating is Haliade-X, with a rotor diameter for 220 meter and a capacity of 14 MW [6]. Meanwhile the largest wind turbine launched is the Vestas V236-15.0MW with a rotor diameter of 236 meter, this is an offshore wind turbine with the industry's largest swept area [7]. To get an idea of how big the rotors are reaching, the modern turbine has reached the length of two football pitches, illustrated in *Figure 1-1* with a Siemens Gamesa 14-222 DD [8]. Next to the single rotor from Siemens Gamesa there is an illustration of a multirotor with seven rotors.
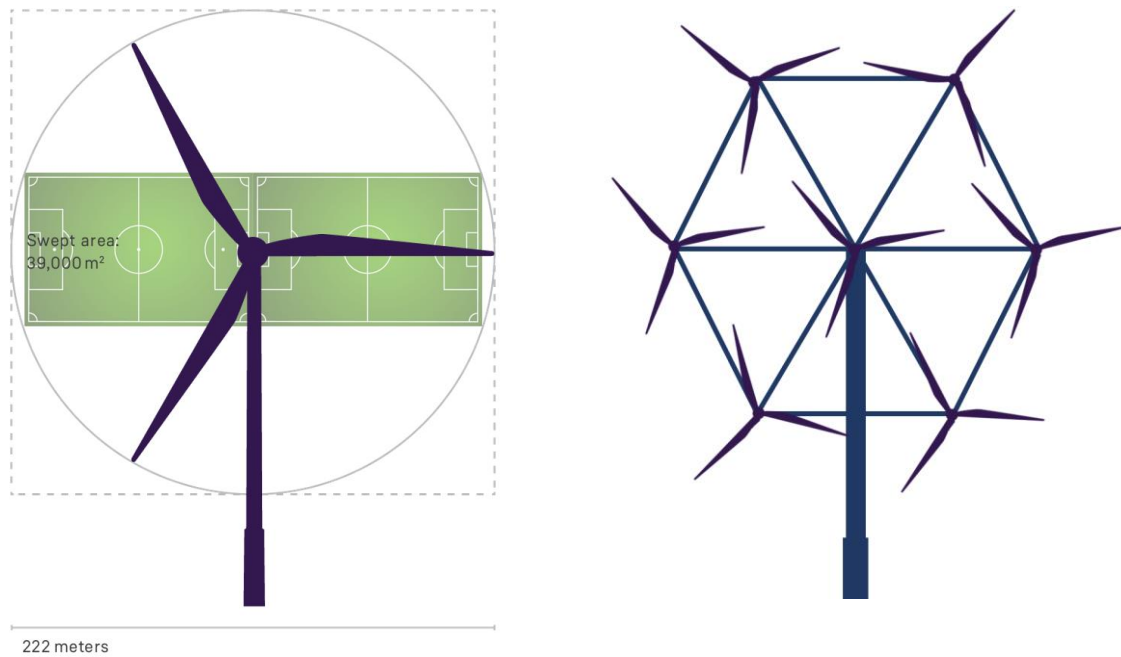
Figure 1-1: Illustration of size compared to football pitches vs Siemens Gamesa 14-222 DD and a multirotor wind turbine (MR7)

Wind power has been a useful energy source for people, in some way, for thousands of years. In the early days it was used directly, such as in graining wheat and sailing boats. In later years, with the rise of electricity, there has been a transition from the more traditional windmills to the modern wind turbines. Even though it is widely accepted by the public to use the term windmill for all rotors harvesting wind, wind turbine is the correct term for the modern type generating electricity. The amount of energy harvested from the turbine is dependent of the incoming wind speed and the swept area of the blades. Over the years the size of the wind turbines has increased in rotor diameter, tower-height, and power output. The increasing diameter-size of wind turbines give new sets of problems, with more complex installation, increasing weight, transportation, pricing, decommissioning and maintenance.

A solution to the problems stated above is to use a multirotor system, composed of smaller but more numerous rotors. The multirotor system is an old idea, but has never had the same success as the singlerotor. In recent years, the interest for multirotors seem to increase, because of the sheer size the singlerotor blades are reaching. With a multirotor system the theoretical power output is unchanged compared to a singlerotor system. With the same swept area and power coefficient, will this count for the power output on a real multirotor? The downside is that there are no viable options for multirotor systems on the market today, but there are some prototypes available for testing purposes. Multirotor in the society may be met with doubt, but possible advantages with weight, cost and installation should be strong arguments for considering multirotor. Today, an argument against wind turbines is the noise. With a multirotor the numbers

of components increases, this leads to the question if the noise will become a larger obstacle? This will need further research before a conclusion can be made. The cost and installation are also a potential advantage, but this will need more extensive data for any conclusion. Decommission will be more manageable due to the reduction of blade size, and the main problem for the offshore wind turbines is the cost, time, and environmental impacts [9]. The large size of the blades requires heavy lift vessels which is expensive [10], and post decommission is problematic due to the storage of the blades [11].

There will also be disadvantages with multirotors compared to the singlerotors with the increased support structure that will cause a greater drag force on the turbine. This has led to the question: How much does the support structure increase the drag, and is there an optimum distance between the discs that will lead to greater power output? This is what this thesis will focus on, and to answer the question above, several experiments on different MR-setups and SR-setups will be conducted.

2. Theory

A multirotor wind turbine uses the kinetic energy from the wind to extract power. In a small-scale experiment it is beneficial to observe a simple one-dimensional (1D) model of an idealized rotor as a non-rotating actuator disc. This simplification enables the small-scale experiment to find the drag forces working on a multirotor.

2.1 Extracting energy from wind – 1D momentum theory

Wind is a powerful natural resource that humans have been exploiting for many years, for example with sailing or windmills. Windmills used the wind to drive a millstone mechanically, but today wind turbines are used for generating electricity. Wind turbines converts kinetic energy from wind to electric energy, which can be used in more distant regions. From the formula for kinetic energy, the power formula can be derived, which makes it possible to calculate the power extracted from the flow through a wind turbine. To obtain the wind turbine's calculated electric output, an efficiency coefficient, called the power coefficient, must be added to the equation, formula (1).

$$P_{out} = \frac{1}{2} C_p A \rho u^3 \qquad\qquad (1)$$

The outgoing wind, in addition to reduced velocity, experience a more turbulent flow than the incoming, caused by mixing of the wind passing the turbine. This flow is called a wake flow and is an important factor to have in mind when dealing with more than one wind turbine, such as in a wind farm. If the wake is not accounted for, the performance of a downstream turbine could be much lower than anticipated. Increased fatigue loads on turbine blades have also been observed in downstream turbines because of the more turbulent wake flow [12].

To calculate the forces on a multirotor by performing a small-scale experiment, 1D momentum theory uses an actuator disc to model a turbine, which will be described in the following chapter **2.2**. It assumes a frictionless, incompressible, and stationary flow around the disc. When using this theory, it opens for valuable insight to the mechanisms of a turbine, and it predicts thrust and power generated. It describes the outgoing velocity of wind harvested by a turbine. As shown in the bottom graph in *Figure 2-1*, the pressure spikes just before passing the disc. Just after passing the disc there is a drop in pressure. Given time the pressure will return to normal. It is also apparent that the wind velocity decreases after passing the disc, due to the extraction of kinetic energy. The theory gives a theoretical ratio for the most efficient extraction and through flow. This ratio is called Betz limit, from the German physicist Albert Betz, and is set to 16/27 and is approximated to 59%.
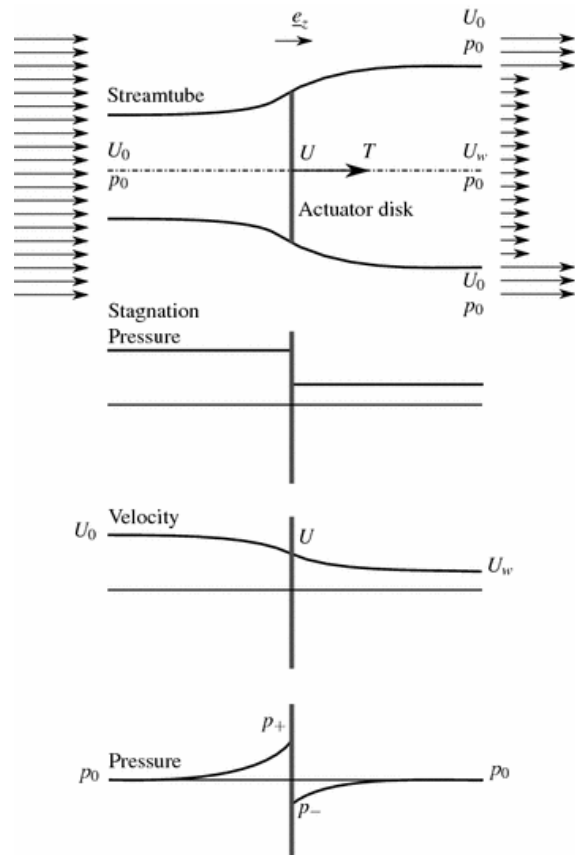

Figure 2-1: 1D momentum theory showing different forces relative to the actuator disc

2.2 Actuator disc

A modern wind turbine is usually composed of three blades with an aerodynamic shape that generates a lifting force. The lifting force sets the blades in motion, causing the turbine to start rotating. In small-scale experiments, an actuator disc also called a permeable disc may be used in place of the rotating rotor. To clarify, this is a circular plate with holes for the fluid to pass through. The permeable disc is modelled to have the same drag coefficient as the rotor it is representing. This is managed by varying the size of the holes, porosity, and disc thickness. The actuator disc will simulate a rotor as seen in ***Feil! Fant ikke referansekilden.Feil! Fant ikke referansekilden.***.
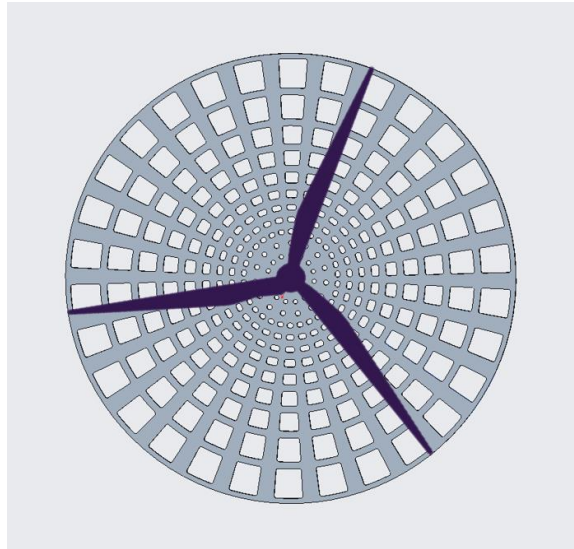
Figure 2-2: Rotor represented as an actuator disc

An actuator disc allows the flow to pass through while it is subject to the influence of the surface forces [13]. The model is based on the conservation of mass, momentum, and energy, which is the main components in 1D momentum theory. The actuator disc is considered ideal as a simulation of a rotating rotor because it is frictionless and there is no rotational velocity component in the wake. It also reduces the velocity of the stream, which causes drag. [13] To calculate the drag on the disc or a general body, a dimensionless drag coefficient is used. The drag coefficient varies with different models and shapes. This will be explained further in chapter **2.3**.

2.3 Drag force

Drag forces appear in any object moving through a fluid and can in aerodynamics be as resistance. It is a force that acts opposite of the relative incoming wind speed and is dependent on the aerodynamic qualities of the object. Drag force can be simplified into two subcategories, skin friction and form drag. *Figure 2-3*: Illustration of form drag and skin friction shows that the type of dominating drag force corresponds with the shape of the object. The form drag is very dependent on the shape of the object, while the skin friction is mostly affected by the shape of the boundary layer.

Shape and flow	Form Drag	Skin friction
	0%	100%
	~10%	~90%
	~90%	~10%
	100%	0%

Figure 2-3: Illustration of form drag and skin friction.

The equation for drag is linked with the Reynolds number, and makes it possible to scale up to full size. In the equation for drag (2) ρ is the density of the fluid, u is the incoming velocity of the fluid, C_d is the drag coefficient, and A is the surface area of the object facing the incoming fluid.

$$F_d = \frac{1}{2}\rho u^2 C_d A \qquad (2)$$

Drag caused by the support structure will be the factor that varies in comparison with a singlerotor. The support structure that will hold the rotors in a MR needs to be strong enough without being too large.

The drag coefficient, as mentioned earlier, is a dimensionless factor that is based on both form drag and skin friction. Regularly the Cd is estimated through empiric data, because it varies with different shapes and Reynolds number, and will be different for a cylinder and a disc.

2.4 Blockage effect

When rotors are placed close to each other, it occurs a blockage effect. The blockage effect gives a lower speed but higher force for a turbine due to the influence of surrounding structures or environment. This can happen in a wind farm or in a tidal range in shallow water. There are three ways to categorize blockage: local, array and global blockage. Local focuses on one rotor in a farm, range, or MR-system. Array is for the flow through the entire farm. Global is for the ratio of channel area to projected area covered by turbines. For a MR, the local blockage will be higher for the

centre turbine in an MR7, and lower for the surrounding turbines, making it possible for its efficiency to exceed the Betz limit [14]. For the global blockage this will not influence the effect considerably if the area outside of the surrounding turbines is infinite, because this will level out due to the lower efficiency of the outer turbines. There may be a greater fatigue on the centre turbines due to this effect. The blockage effect is investigated in an article by Nishino and Willden, where they tested to find an optimum spacing between the turbines in a tidal array. By placing rotors close enough there will occur a local blockage that slows the velocity. They discovered a local increase in Betz' limit due to the blockage, increasing to 0.798. [14]

2.5 Multirotor Wind turbines

The concept of a multirotor is that it has the same swept area as a singlerotor but has a different amount of turbines. With a multirotor wind turbine, you split the swept area into smaller sections which add up to the same area as a singlerotor, the number of rotors needed is shown in equation (3). There are numerous advantages with the multirotor concept, such as reducing costs, installation complexity, and total weight may be influenced by using smaller and more numerous turbines. Transportation and maintenance are also possible advantage points, with smaller blades being easier to transport, and being able to still run parts of the MR during maintenance. This leads to the MR still generating power, and keeping a more stable flow of electricity, even during downtime for some of the rotors. Today there are no competitive multirotors on the market, but there are some prototypes. Vestas have built a full scale multirotor in Denmark, with 4 rotors [15], which is mainly used for research purposes.

$$Number\ of\ multirotor\ turbines = \frac{Area\ of\ singlerotor}{Area\ of\ one\ rotor\ in\ a\ MR\ system} \qquad (3)$$

The main difference between singlerotor turbines and multirotor turbines are the number of rotors per structure. The singlerotor is a large structure with huge blades driving a single generator. This may cause problems when it becomes too heavy for the structural material to sustain [9], and is when the multirotor can be a substitute. There are more components in a multirotor system, but the components are smaller and lighter. In the end this may make the multirotor setup lighter and with roughly the same power output. The equation for power output has one variable that is controlled by the structure, this is the swept area of the blades. If the swept area of the turbines is the same, it should not be any loss in the power output due to having

multiple rotors. A turbine with four rotors costs approximately 15% less to construct than a turbine with one rotor, even though the blades cover the same area in total [16].

2.6 Scaling

When testing a wind turbine, there is a need to make models due to the huge size off a full-scale turbine. To complete a small-scale experiment the construction needs a scaling factor. If the full-scale wind turbine has a diameter of 200 meters and the test model 0,2 meters, the scaling factor would be 1000. This is the geometrical scaling and shows a constant difference in size. However, different fluids can be used to get testing conditions as similar as possible to full-scale. To conduct an experiment with an actuator disc in water compared to a wind turbine in full-scale, it is necessary to apply scaling laws that ensures the similar behaviour.

There are different dimensionless coefficients which can be used as a scaling variable, such as Froude-, Mach- and Reynolds number, and these make it possible to use scaling. When a body moves through a fluid, the forces that arises is inertia, elasticity, and gravity. These forces are directly represented by the various terms from the Navier-stokes equation. The gravity force is the force working on the fluid, and not on the body. When testing drag on a low-speed component in water, it is possible to compare results with a full-size model by matching Reynolds number. This coefficient is used because the model is stationary during testing. If a model experiment has about the same Reynolds number as the full-scale application, the model and the full-scale flows will be dynamically similar. The Reynolds number contains inertia force divided by viscous force as seen in equation (7). [17]

$$F_d = \frac{1}{2}\rho u^2 C_d A$$

(4)

$$Inertia\ force = \ pl^2 u^2$$

(5)

$$Viscous\ force = \ \mu u l$$

(6)

9

$$Reynolds\ number = \frac{inertia\ force}{viscous\ force} = \frac{\rho}{\mu}ul \qquad (7)$$

Reynolds number can be used in scaling due to being dimensionless. Density, viscosity, velocity, and area are the components for calculating the Reynolds number. Velocity is the main changing factor over time. Density, viscosity, and area for the most part static and will not change after installation. Most experiments take place in labs without the spacing required to test full-scale. For instance, the modern wind turbines have breached the 200 m diameter mark, which makes testing inconvenient. By changing the fluid used in testing to something more dense and less viscous, gives the opportunity to make the test object smaller, and still getting around the same Reynolds number.

Given these circumstances it is simpler to use scaling. Air has a lower density and viscosity than water, so by using a smaller area and a lower velocity in water, it is possible to use scaling. Equation (8) shows the Reynolds number for full scale. Equation (9) shows the Reynolds number for full scale in water and equation (10) shows Reynolds number for small-scale in water. The velocity in equation (8) 12 m/s was chosen due to being standard rated wind speed among full-scale wind turbines. The size of the wind turbine is set to 150 m, which is a normal industrial size, and a little smaller than the largest turbines.

$$Re_{Fs} = 1.23 * 10^8 = \frac{1.225\frac{kg}{m^3} * 12\frac{m}{s} * 150m}{1.8 * 10^{-5}\frac{Ns}{m^2}} \qquad (8)$$

$$Re_w = 7.5 * 10^7 = \frac{1000\frac{kg}{m^3} * 0.5\frac{m}{s} * 150m}{1 * 10^{-3}\frac{Ns}{m^2}} \qquad (9)$$

$$Re_{ss} = 1 * 10^5 = \frac{1000\frac{kg}{m^3} * 0.5\frac{m}{s} * 0.2m}{1 * 10^{-3}\frac{Ns}{m^2}} \qquad (10)$$

3. Method

In this project there will be a theoretical approach and an experimental part. The theoretical approach contains calculations for drag, Reynolds number, and drag coefficient, and these results will be compared with results from the experiments conducted. The results from both approaches will be placed into tables or graphs for an easier comparison between them. Reynolds number will from now on be measured for a single disc with a diameter of 20 cm as reference.

3.1 Theoretical approach

The theoretical method is a calculation of all drag forces on a MR-structure + support. It contains an excel sheet with all the components chosen for calculating the drag forces, in **Attachment 1**. The aim for the theoretical approach is to estimate the drag forces the MR-system will be exposed to during the testing. A multirotor should, with the same conditions, only get slightly higher forces compared to a singlerotor due to the increase in support structure area. The explanation for this is that the drag force equation does not account for any small variables that may distinguish the two approaches. For instance, the blockage effect, the shape of the MR system, and the boundary conditions are some of the variables that the force equation does not differentiate.

The equation and variables for drag in a fluid were determined to find the theoretical approach for the drag forces influencing a multirotor. The equation was derived in chapter **2.3**. A thing to notice is the area of the support structure will be calculated as a rectangle, due to the cross-section of the cylinder pipes facing the incoming fluid. The drag force was calculated for the disc and support structure separately, and multiplied with the corresponding number of discs, and structures. By summing up the drag for the discs and support structures the result will be a sum of total drag for the MR-system, seen in equation (11). The first calculation was the theoretical drag forces that the structures were exposed to. There were calculations for each model with the three different distances between the discs, and with different velocities.

$$F_{d,total} = \sum F_{d,Disc} + \sum F_{d,Support\ Structure} \qquad (11)$$

Furthermore it was debated how much of the support structure should be used to calculate the drag forces, since parts of the support structure is set behind the disc and would not be exposed freely for incoming velocity. For this case, the whole length of the support structures was used, since the values and differences are small. The values are also used for comparison, meaning that how the values change according to each other are more important than exact values. The length of the support structures will be discussed more in chapter **5**.

There has also been calculated drag forces for different MR-systems, with only changing numbers of rotors. A total drag coefficient was also calculated by restructuring the formula for drag. For an estimation of force, the drag coefficient of the actuator discs was initially set to a value of 0.82, from Karlsen and Sætrans experiments from 2019 [18], because of the matching area of Reynolds numbers at 10^4-10^5.

3.2 Experimental method

The experiment was conducted in the Marin Lab at Western Norway University of Applied Science in Bergen. The model was dimensioned by the theoretical forces calculated in the theoretical part. This was a small-scale experiment determining the drag forces that will be compared with the theoretical results.

3.2.1 Marin Lab

The experiment took place in the Marin Lab which consists of a large tank with water and a carriage that runs over the tank. The tank dimensions are 50 m long, 3 meters wide and 2.2 meters deep, and is considered large enough for the MR experiment. The carriage is built like a rig where different equipment can be fixed or installed. To run the carriage there is a control panel connected to a computer where the speed and position can be chosen.

As mentioned, changing the fluid can be used as an action taken to handle scaling, such as changing the fluid from air to water. The reason why this is possible is described in chapter **2.6.** The benefit of using water for this experiment was the easy access of a water tank, the testing requires less energy, and generates less noise than in a wind tunnel. Ideally, a full-scale test would have been done, but as mentioned earlier, the sheer size of models makes it difficult. It would have been interesting to have the test models in a wind-tunnel, to see if the results would have been any different. The tank with the rig is shown in *Figure 3-1*.

Figure 3-1: Experimental tank at the MarinLab with the carriage

3.2.2 **Model design**

In preparation of the experiment several MR setups were considered from both the report of the wind energy conference in Cork [19], and through a brief creative workshop within the group. The final decision was to use a MR7 with a hexagonal structure, and a MR4 with a squared structure as shown further down in *Figure 3-10* and *Figure 3-11*. The experiment needed a support structure to combine the actuator discs, and the structure used for this model is shown as a CAD sketch in *Figure 3-2* and *Figure 3-3*. The support structures are shaped as a hexagon with pipes going into the centre, and as a square with a cross in the middle. For time and material reasons, it was not possible at the given time to test MR-systems with more than seven discs.
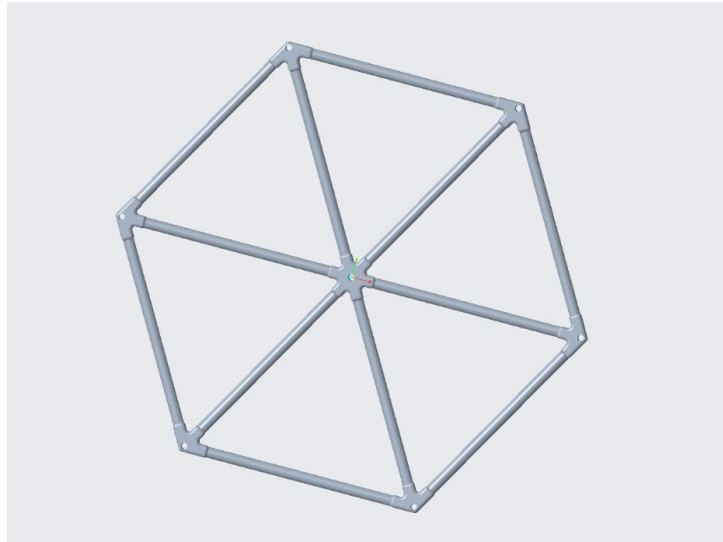
Figure 3-2: CAD sketch of support structure for MR7
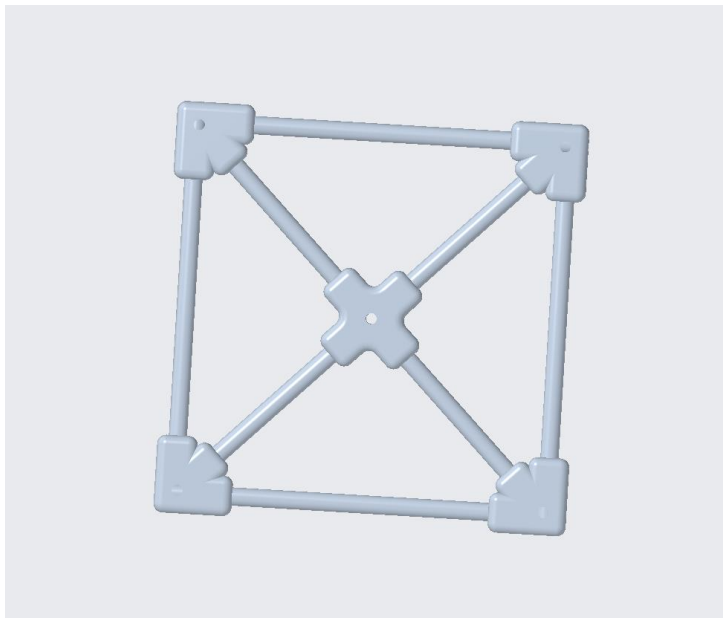
Figure 3-3: CAD sketch of support structure for MR4

The design included self-designed plastic joints to connect support structure and discs to each other. For the structure, 10 mm diameter pipes of stainless steel (4401) were assumed to be strong enough, according to the forces that was calculated in the theoretical approach in chapter 4.1. The plastic joints were designed in Creo and exported as a Stereolithography file, to be used in the printer Flash Force Adventure 3, through the printer program Flash Print. First there was made a test-model in Creo which was printed, to check if the connector-sizes were adequate. A 10 mm test pipe was used to test the tolerance of the connector, and later in a destructive test to check the strength of the joint. The tests were repeated with adjusting the cad model, until the

pipe fit the holes, and the module was tough enough, and ready for production. The inside diameter of the joint connectors for the pipes was set to 10.3 mm and the hole to attach the disc was set to 6 mm. To make sure the strength of the 3D part was sustainable the infill was set to 25% and verified by the destructive test. Images of the CAD-drawings of the joints are shown underneath in *Figure 3-4* and *Figure 3-5*. The CAD drawings can be found in **Attachment 2**.
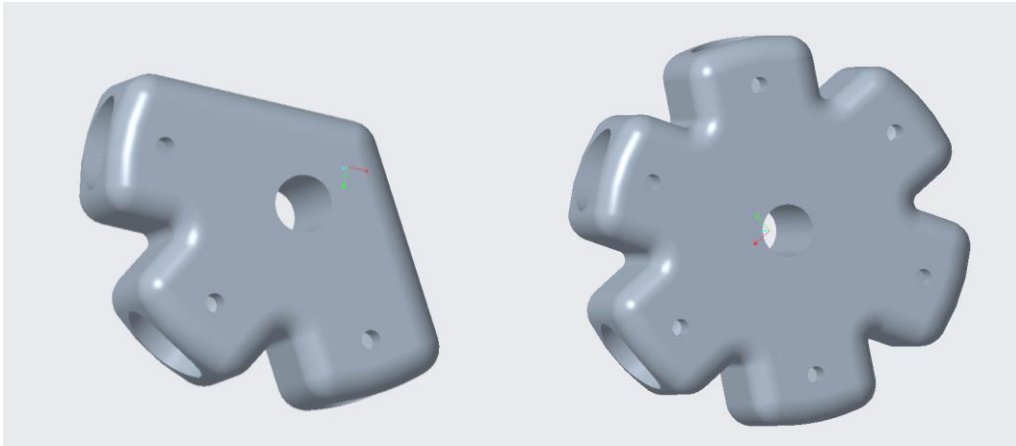
Figure 3-4: CAD drawing of connection joints for MR7
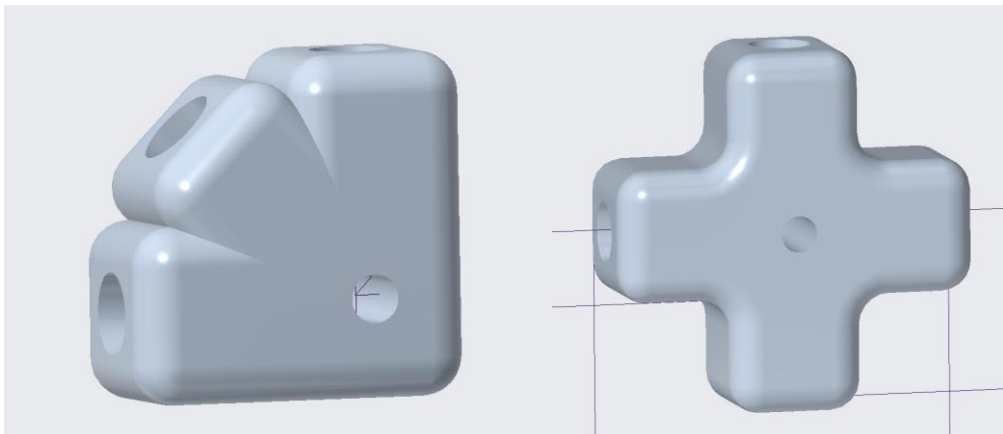
Figure 3-5: CAD drawing of connection joints for MR4

3.2.3 **Experimental model**

The experimental model for the MR7 involved seven actuator discs, twelve pipes and six joints for the sides in the hexagon, and one joint for the middle. The MR7 was built with three different distances between the discs. The chosen distances were 1.0, 1.1 and 1.4 diameter. 1.0 diameter means that there is one diameter from the center between to discs. The MR4 model involved four discs, eight pipes, four outer joints and one centre joint. The distance between the discs in the MR4

is 1.1 diameter. All parts for building the MR7 is shown in *Figure 3-6*, and *Figure 3-7* shows the finished support structure and the actuator disc ready to be assembled together.
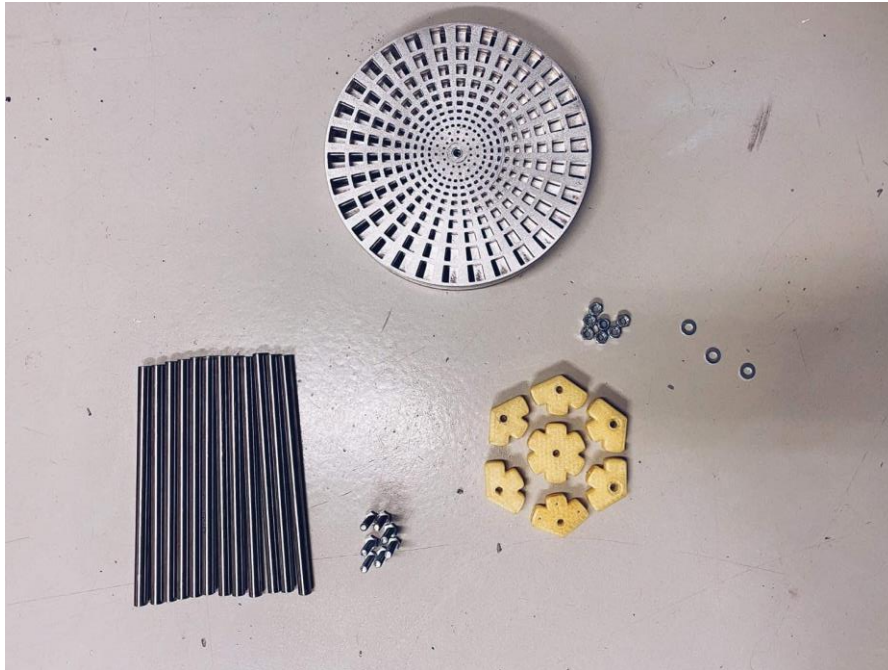

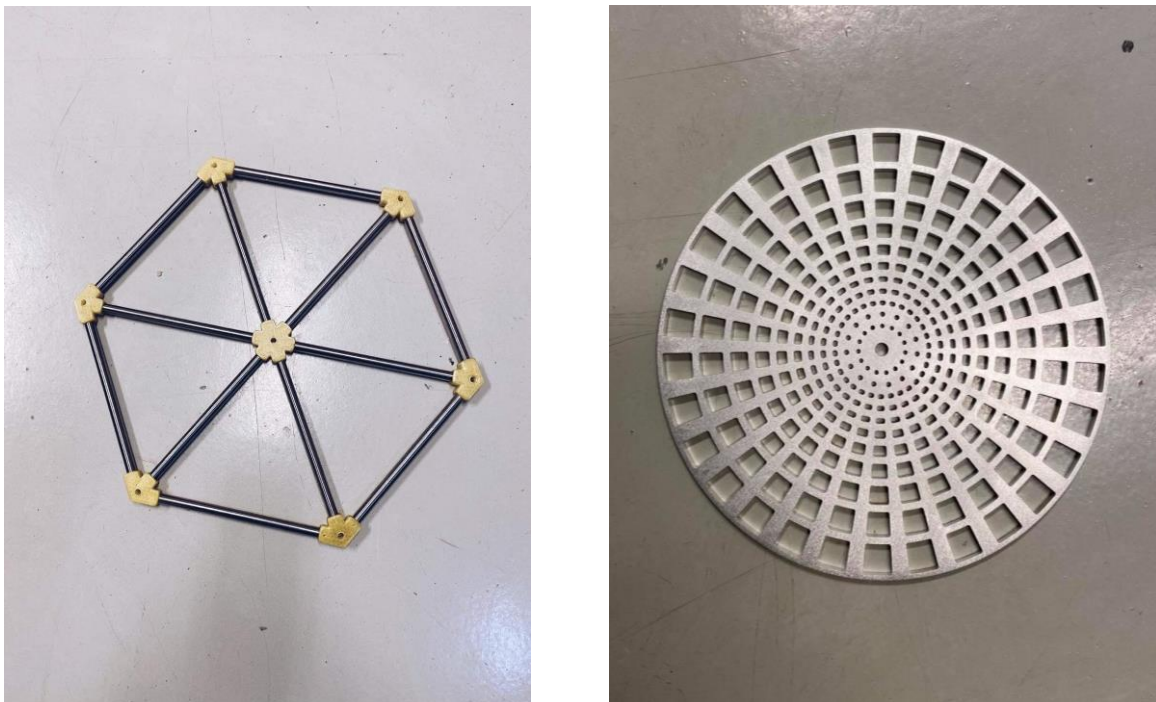*Figure 3-6*: Construction parts for the multirotor model

Figure 3-7: Structure and actuator disc

The solidity of the actuator disk is calculated by equation (12) using the dimensions of a 60 cm actuator disc, this will make no difference since the 20 cm disc is structural the same, with a scaling factor of 3.

$$\frac{161495\ mm^2}{\pi * (600\ mm)^2} = 0,1428 \approx 14,3\% \tag{12}$$

Picture of the experimental model, MR7 1.0D is shown in *Figure 3-8* from both sides to see how the support structure is connected. *Figure 3-9* shows the MR7 1.0D and the SR 60 cm compared next to each other.
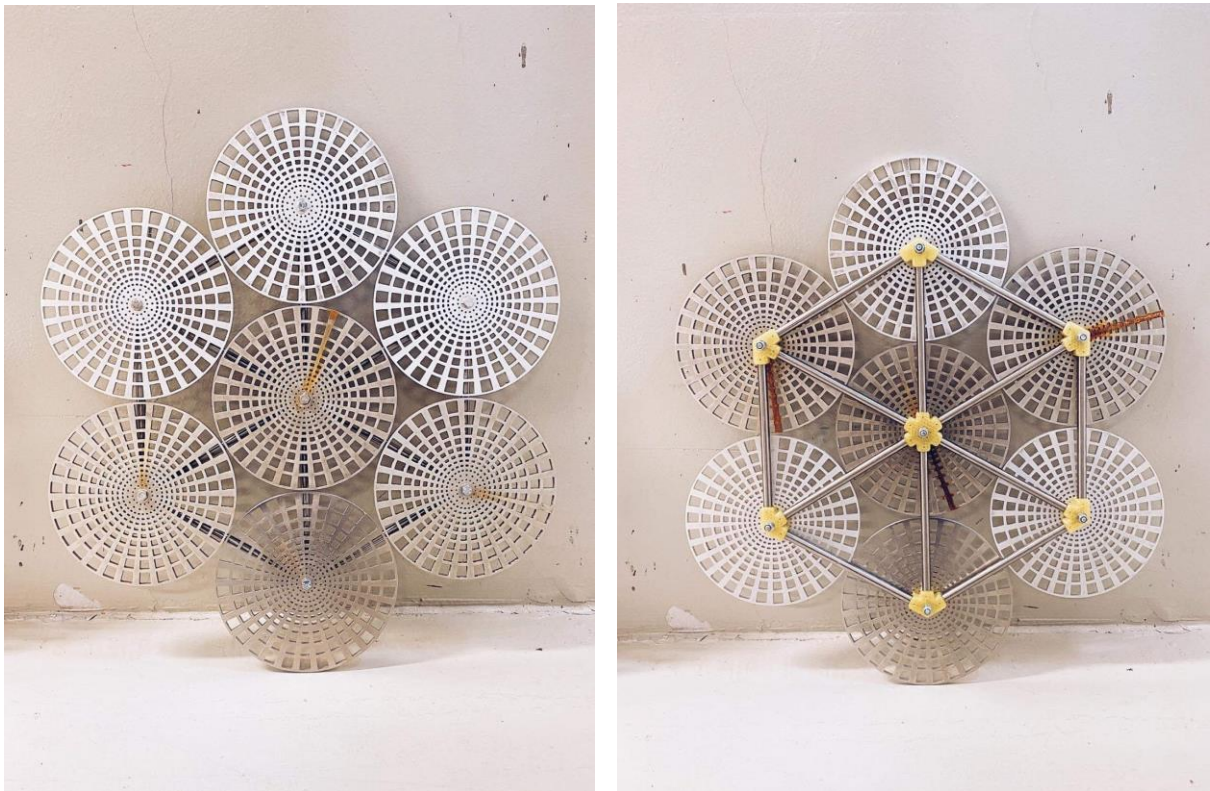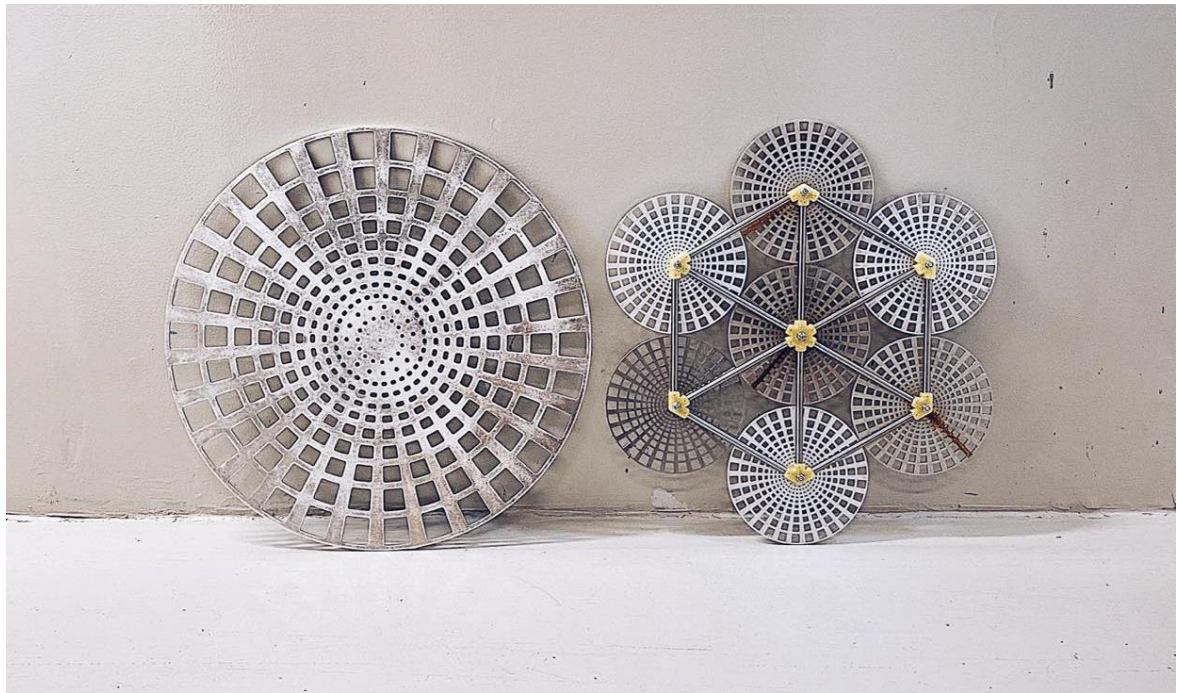

Figure 3-8: MR7 1.0D test model

.

Figure 3-9: SD 60 cm and MR7 1.0D

The MR7 setup is presented in *Figure 3-10* to compare the three different distances. The 1.4D is missing the outer pipes for the pictures, but it was connected while testing. *Figure 3-11* shows the MR4 setup with the distance 1.1D that was tested.
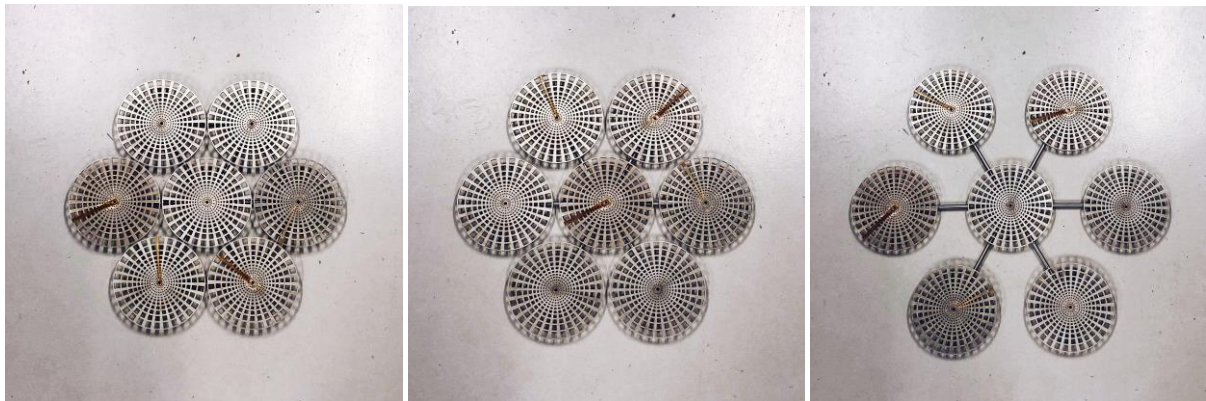
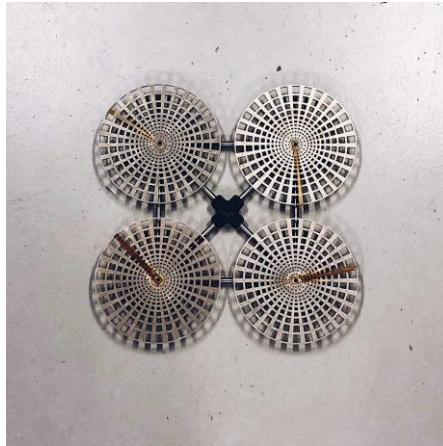*Figure 3-10*: MR7 setups with the different distances 1.0D, 1.1D and 1.4D

Figure 3-11: MR4 setup with 1.1D

3.2.4 **Load cell**

Testing started with preparations and calibration of the load cell. The drag force can be simplified as the forces acting in the x-axis, along the tank, which can be read from a load cell. The spreadsheet gave an estimate of around 30 N for the MR7 setup, so initially a 50 N load cell was chosen. Unfortunately, the 50 N load cell was damaged in the preparations, and a 100 N load cell had to be used instead, seen in Figure 3-12.
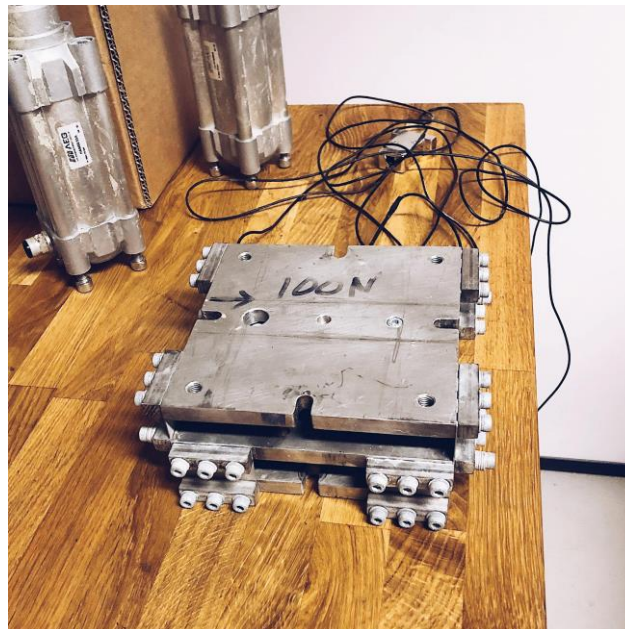

Figure 3-12: 100 N loadcell

The calibration was performed by applying a known load and take the voltage-readings from the program Lab View and inserting it in an Excel spreadsheet. The calibration took ten measurements, increasing stepwise with five loads and then decreasing with the same five loads

as shown in *Figure 3-13*. From the spreadsheet the gain and offset were calculated and was inserted in Lab View for further use. A hysteresis diagram was formed to check if the measurements were good. The coding in Lab View was set up by the lab-engineer due to lack of competence from the group, and technical difficulty of the program.
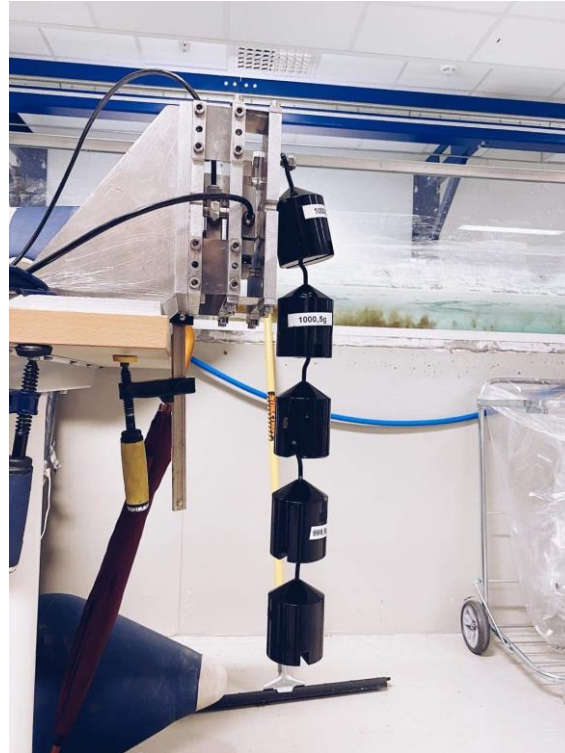

Figure 3-13: Calibration of load cell. Five known loads applied

3.2.5 Load force measurement

A load cell is a force transducer that converts a force into an electrical signal that can be measured. The conversion happens in a strain gauge which is a stretch flap inside the load cell. As the force applied to the load cell increases, the electrical signal changes proportionally. The load cell can only take up forces along one axis but can be combined to measure in two dimensions.

3.2.6 Test setup

Before the tank-testing could begin, some modifications to the rig-setup had to be applied. The load cell was mounted on a structure that was fixed to the rig and tightened with screw clamps. Making it the only connection between the rig and the structure holding the MR-system. To fit the MR-system to the load cell, a steel pole was attached to a beam, with the beam mounted on top of the load cell. The middle attachment point of the MR-system was fitted with a longer screw, so it could go through the attachment, the disc, and the pole, with a nut fitted at the back. The pole was

also fastened with cable tie to the support structure, to minimize movement. The discs were then attached to the MR-system, and the setup was ready for testing.

If there are boundary conditions like walls, turbines next to each other, or a channel the system will go from 1D to 3D. This experiment is performed in a tank with walls and floor, and this may have had an impact on the results, since 1D momentum theory is the base for the actuator disc. To minimize the impact of the boundary conditions, some considerations was applied such as keeping the MR-system as far from the boundary layers as possible. A tank-width of 3 m, the structure being 0.6-0.76 m, gives a clearance between the structure and walls of around two diameters on each side.

The rig uses a carriage that was towed over the testing tank. The carriage can hold a lot of weight and can easily hold two people on top as they are preparing the rig. The velocity of the rig can be altered to fit the test, and QR-codes fitted on the wall is scanned by the rig to map its position. Depending on the testing, different analysis tools can be applied to the rig, such as the load cell in this case. The rig setup is shown in *Figure 3-14*.
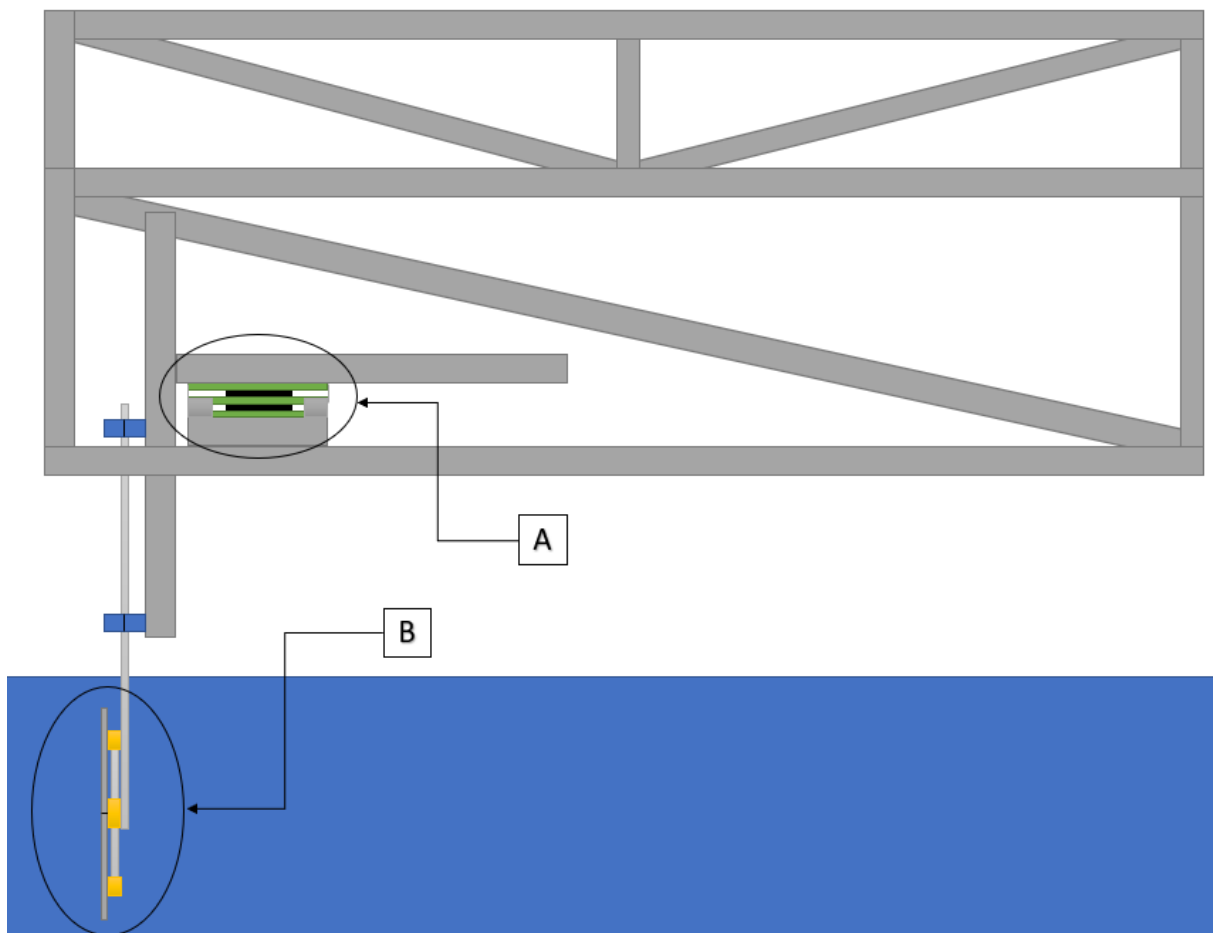

Figure 3-14: Rig, the load cell is placed at point A, and the disc is placed at point B.

3.2.7 Testing and data gathering

To gather data from the testing the program Lab View was used for reading the measurements from the load cell. This only required to start and stop a recorder, while the rig was going back and forth in the tank. For each of the different speeds and distances between the discs, approximately five runs were chosen to have quantitative measurements. This gives a total of around 125 runs per structure, for better mean value and error estimation. After the first MR7 had gone through the testing, the number of runs with velocity at 0.1 was shortened to three per structure, due to the high amount of output data. During the testing, it was attempted to start and stop the carriage while it was at a steady pace. The reason for this is that during acceleration the forces on the MR-system will be more unstable, and therefore not be comparable to the forces for a carriage running at constant speed. *Figure 3-15* shows the MR7 during testing.

Figure 3-15: MR7 during testing

The data from the testing were exported as .txt files, and Lab View treated the data so it would be ready for plotting.

3.2.8 Data analysing

By using available MATLAB plots the data was generated, and some codes made it possible to present the graphs from the data. After plotting the result there were one graph with the drag and velocity and one graph with the drag coefficient and the Reynolds number for each of the different structures and distances. The graphs for the same setups were then put together in a combined

graph with error bars, which shows the standard deviation to easier make comparisons. The graphical illustration from MATLAB made it simpler to analyse the results. **Attachment 3** shows one example of the codes used.

3.3 Potential errors

Under each point, a small discussion explains why the point was considered a source of error, and what was done to reduce the amount of error in *Table 3-1*. This does not take in consideration systematic errors such as wrong usage of code in MATLAB, or program bugs.

Source of error	Measures taken
Carriage-rail causing vibration	Since using average values this does not have a big impact.
Measuring inaccuracies from load cell	Repetitive measurements to minimize impact of single measurements.
Error calibration of the load cell	Repetitive calibration
Start and stopping of measurements to early/late could provide wrong data due to the acceleration forces are different then the steady pace forces.	Close attention at the start and end of carriage run-time, to start and stop at the correct time. Review and cutting of time series in MATLAB
Tilting the pole holding the MR-system while running underwater, and structure flexing	Tightening the pole to the rig at two points and using a hard material. Used over-dimensioned infill on plastic joints. Visual verification that the tilt angle is low.*

Table 3-1: Source of error

*A low tilt angle gives a minor decrease in the drag force. For instance, an incoming force of 10 N hitting a MR with tilt angle of 3°, gives a decomposed force, Fx, of 9.986 N from formula (13).

$$Fx = Cos(3°) * 10\,N = 9.986\,N \qquad (13)$$

4. Results

The results are divided into two parts, the theoretical results from calculations, and the experimental results from testing different models.

4.1 Results from theoretical calculation

The theoretical calculations are the foundation to estimate how much forces the models need to withstand during testing. The calculations also give numbers to compare with the experimental test results. The formulas used is in this comparison are simplified as they do not take interactions effects such as blade age between the single discs in a MR into account. For the initial calculations, a drag coefficient of 0.82 was applied, as mentioned from Karlsen and Sætran [18]. The drag coefficient will later be substituted out with a coefficient from the experimental part, which will be used in further calculations and comparisons. The drag coefficient for the pipes was estimated to be 1.1, from a graph showing different C_d values for cylinders with different Reynolds numbers, with a Re estimated to be around 100 000 during the testing [20].

Table 4-1 shows the total drag calculated for the different velocities and distance between the discs. The total drag is a sum of the drag from the support structure added with the drag from the discs, with a disregard from blockage effects. The calculations shows that there is a small increase in drag between 1D and 1.1D. Between 1.1D and 1.4D there is a larger change, this is expected due to having larger cross section of the support structure exposed to the flow. The full table is seen in **Attachment 1**. For the drag coefficient used in the theoretical calculations, the coefficient results from the experimental SD 20 cm in **4.2.7**, setting the C_d to 0.87. The reason for this is that it gives a more applicable drag coefficient, since the multirotors was tested at the same tank, with the same setup.

Fd total [N] MR7					
			Distance between discs [D]		
			1.0	1.1	1.4
Velocity [m/s]		0.1	1.09	1.10	1.14
		0.2	4.35	4.41	4.56
		0.3	9.79	9.91	10.3
		0.4	17.4	17.6	18.3
		0.5	27.2	27.5	28.5

Table 4-1: Total drag force MR7

Table 4-2: Total drag force MR4 is the theoretical drag calculations for MR4. For this model there is a slightly smaller growth between the discs than for the MR7. This is expected due to the smaller area factor in the formula (2) for drag. Even though the overall values are a bit lower than for the MR7, it follows the same pattern, with increasing values for longer distances between discs, and higher velocities. When comparing theoretical and experimental, only the MR4 1.1D will be compared, since it was the only setup tested for the MR4.

Fd total [N] MR4				
		Distance between disc [D]		
		1.0	1.1	1.4
Velocity [m/s]	0.1	0.63	0.64	0.67
	0.2	2.54	2.57	2.68
	0.3	5.71	5.79	6.03
	0.4	10.1	10.3	10.7
	0.5	15.9	16.1	16.7

Table 4-2: Total drag force MR4

Since the support structure is what separates the MR from the SR, calculations were made on the support structure alone. *Table 4-3*: Total drag force on only the support structure for different velocities and distances shows the total drag on the support structure of MR7 with different spacing and velocity. The results show, as expected, that the drag will increase with larger structure and higher velocity, because the area and velocity both are changing factors. Since velocity is a squared factor, it affects the drag quadratically.

Fd total [N] Support structure MR7				
		Distance between discs [D]		
		1.0	1.1	1.4
Velocity [m/s]	0.1	0.13	0.15	0.18
	0.5	3.30	3.63	4.62
	1	13.2	14.5	18.5
	1.5	29.7	32.7	41.6

Table 4-3: Total drag force on only the support structure for different velocities and distances

Table 4-4: Total drag force on only the support structure for different velocities and distances shows the force of support structure for the MR4 and follows the pattern from the tables of total drag forces with overall a slightly lower value.

Fd total [N] Support structure MR4				
		Distance between discs [D]		
		1.0	1.1	1.4
Velocity [m/s]	0.1	0.09	0.10	0.12
	0.5	2.20	2.42	3.08
	1	8.80	9.68	12.3
	1.5	19.8	21.8	27.7

Table 4-4: Total drag force on only the support structure for different velocities and distances

There were made calculations of how the drag coefficient acts with the Reynolds number. *Table 4-5*: Drag coefficient for the whole MR7-system. shows a drag coefficient for the whole system, the disc and support structure. It shows that the theoretical C_d will be constant for the different velocities and will only change with the different distance between the discs.

Drag coefficient [Cd] MR7				
Velocity	Reynolds number	T-Cd D=1	T-Cd D=1.1	T-Cd D=1.4
0.1	19990	0.990	1.002	1.038
0.2	39980	0.990	1.002	1.038
0.3	59970	0.990	1.002	1.038
0.4	79960	0.990	1.002	1.038
0.5	99950	0.990	1.002	1.038

Table 4-5: Drag coefficient for the whole MR7-system.

Table 4-6 shows the drag coefficient for the MR4. An interesting finding is that the drag coefficient for the MR4 is slightly higher than for the MR7. At first notice this could be counterintuitive due to the overall lower values of the MR4 in the earlier tables. When looking at the MR4 structures it shows an increase in number of pipe-to-disc ratio, compared to MR7. The drag coefficient is calculated with area as a variable, and the increase of pipe-to-disc value gives an overall higher drag coefficient.

Drag coefficient [Cd] MR4				
Velocity [m/s]	T-Reynolds number	Cd D=1.0	Cd D=1.1	Cd D=1.4
0.1	19990	1.010	1.024	1.066
0.2	39980	1.010	1.024	1.066
0.3	59970	1.010	1.024	1.066
0.4	79960	1.010	1.024	1.066
0.5	99950	1.010	1.024	1.066

Table 4-6: Drag coefficient for the whole MR4-system.

4.2 Results from lab experiments

The results from the experiments are based on the MR7 model, with different distance between the discs and velocities. The data from testing is presented by graphs from MATLAB. The experiment also contained testing the support structure alone, and singlerotors with different sizes. Due to time restrictions, the MR4 and SR had to be tested later than the MR7.

4.2.1   Results MR7 drag vs velocity

Figure 4-1 illustrates the drag on the MR7 with the three different distances. The dots demonstrate the growth in drag with increasing velocity. The formula for drag has a squared velocity factor that indicates that there should be a square growth with changing velocity, this is clearly shown in the graph. This means the calculations matches with the results from the experiment. The drag is reaching a peak point at around 30 N at the speed of 0.5 m/s.
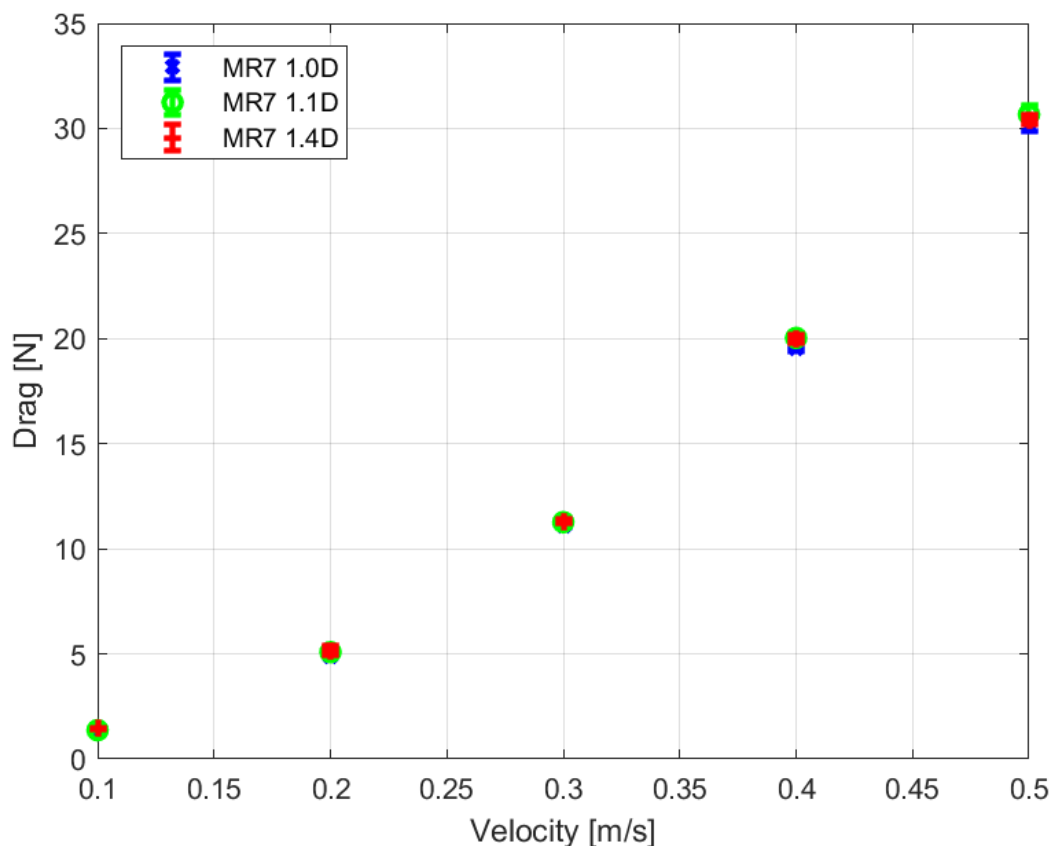
Figure 4-1: Results for MR7 drag vs velocity

Comparing all three distances of the MR, the drag forces increase marginally more between 1.0D and 1.1D, than between 1.1 D and 1.4D. One theory to explain this is the space between the discs

is big enough for the fluid to flow through, which explains why the drag is not increasing even if there is more support structure. When the fluid is passing through the MR some of it will go straight through. This lowers the blockage effect for the MR with 1.4D distance, where the blockage effect will more greatly impact on the discs with smaller distance. Given the differences are within the measurement uncertainty, it may not be a clear conclusion.

4.2.2 Results MR7 drag coefficient vs Reynolds number

Figure 4-2 represents the drag coefficient varying with the Reynolds number. At lower Reynolds number, all the different setups showed a peak in drag coefficient varying in the area 1.15-1.35. When the Reynolds number is larger than 20 000 the drag coefficient starts to stabilise for all the systems at around 1.12.
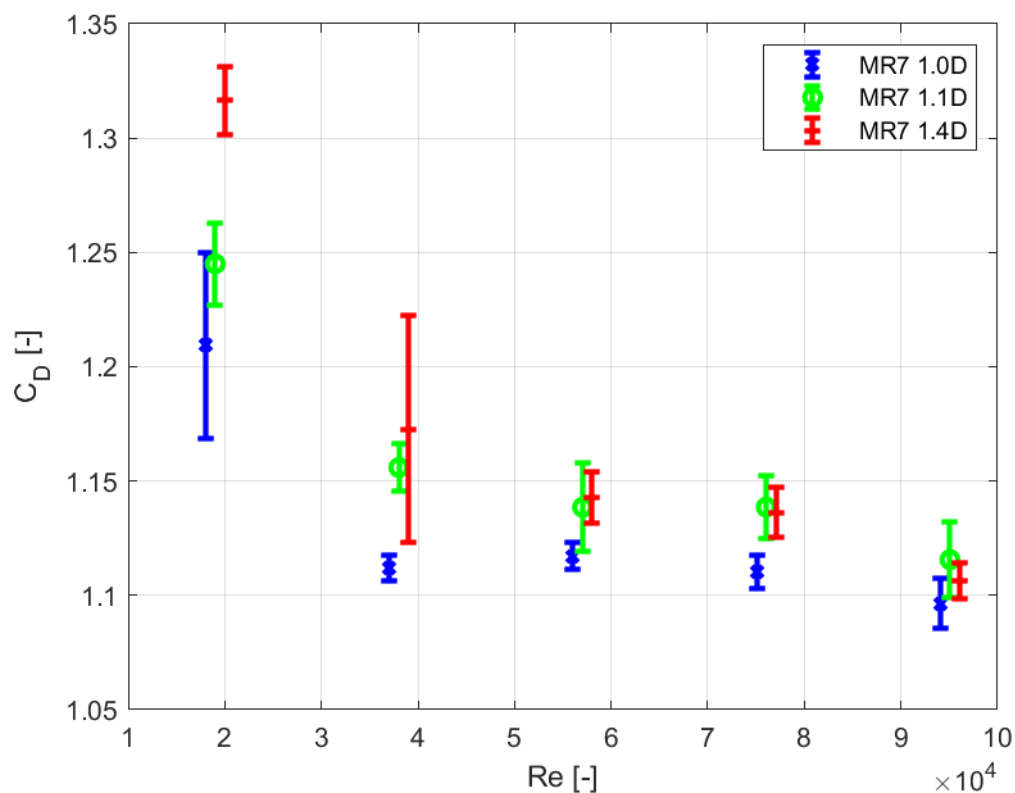
Figure 4-2: Results for MR7 drag coefficient vs Reynolds number

When comparing the different distances, an error bar consisting of the mean value with the standard deviation to make it more presentable. The error bars shows that there will be an overlap on most of the measurements, making it more difficult to separate the different features, because they move within the same uncertainty. On lower Reynolds numbers there is a greater leap on the points for different distances. For larger Reynolds numbers the C_d evens out, and the

error bars stretching over a shorter range. It is used an offset of +/- 10^3 in Reynolds number for two of the distances for the graphical presentation. Overall, the blue points of 1.0D seems to be a bit lower than the other two, yet marginal, and the differences evens out at a drag coefficient around 1.12 from a Re of 40 000. Even though there are some differences between the data from the experiments, the patterns are clear in all three of the cases with a squared trend-line for the drag forces, and a stabilizing of the drag coefficient with an increasing Reynolds number.

4.2.3 **Support structure SMR7**

The support structure was tested isolated without the discs. *Figure 4-3* presents the results for the drag increasing with the velocity. In this case it also appears the same square growth as seen before for the whole MR7-system. The differences between the systems are bigger for the support structures, and the difference increase with the velocity. The MR7 1.4D support structures has the highest amount of drag, and the 1.1D has a minor increase from the 1.0D. The velocity for the support structures was increased during structural testing to make it easier to see the differences between the different setups. Small differences in data points give a narrow representation of results.
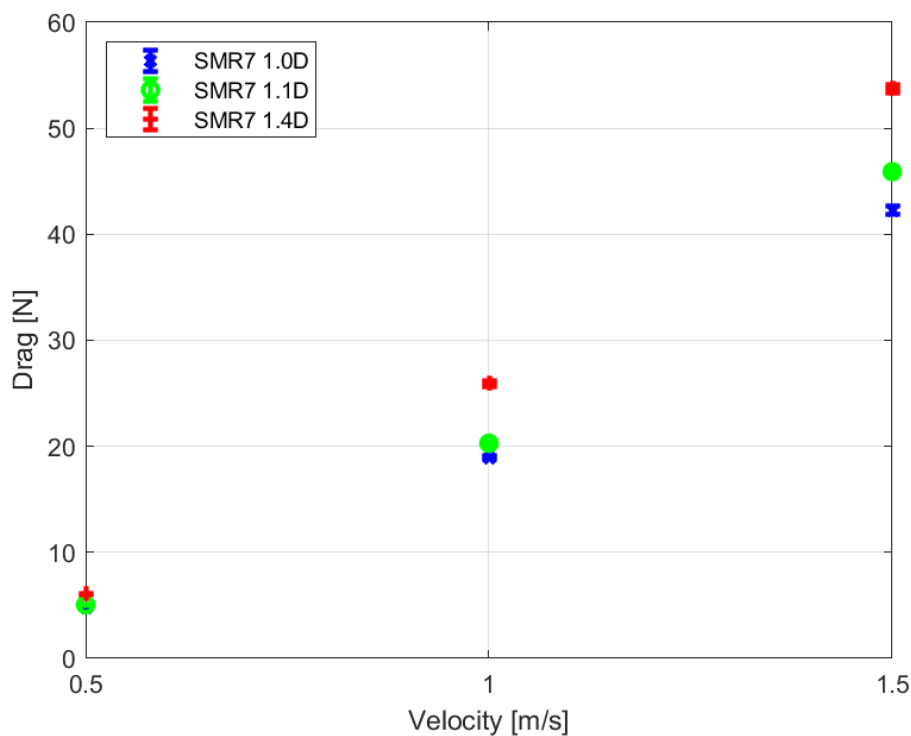
Figure 4-3: Results for SMR7 drag vs velocity

Figure 4-4 shows the results of testing the SMR7 for drag coefficient and Reynolds number. The graph shows a stable drag coefficient for all the measurements, with a small exception of the SMR7 1.4D, which shows some more deviation than the other two. The error bars are relatively small for the support structure compared to the whole MR7-system, and no overlaps gives more valid results to conclude from
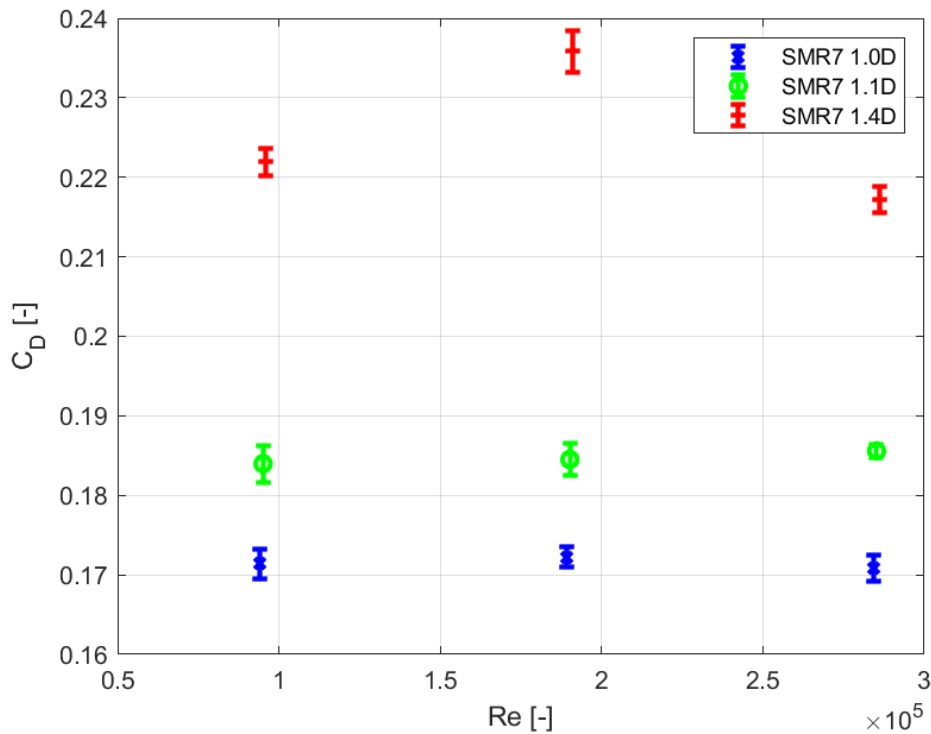
Figure 4-4: Result for SMR7 drag coefficient vs Reynolds number

4.2.4 **Results MR4 drag vs velocity**

The results from the MR4 were tested with the distance 1.1D, seen in *Figure 4-5*. Again, the same trend with the quadratic growth is seen in the results, but the drag is visibly lower than the drag on the MR7. The MR4 reaches a peak just above 12 N, at 0.5 m/s. A difference for the MR4 setup compared to the MR7 setup is the empty space between the discs, which will be discussed in chapter **5**.
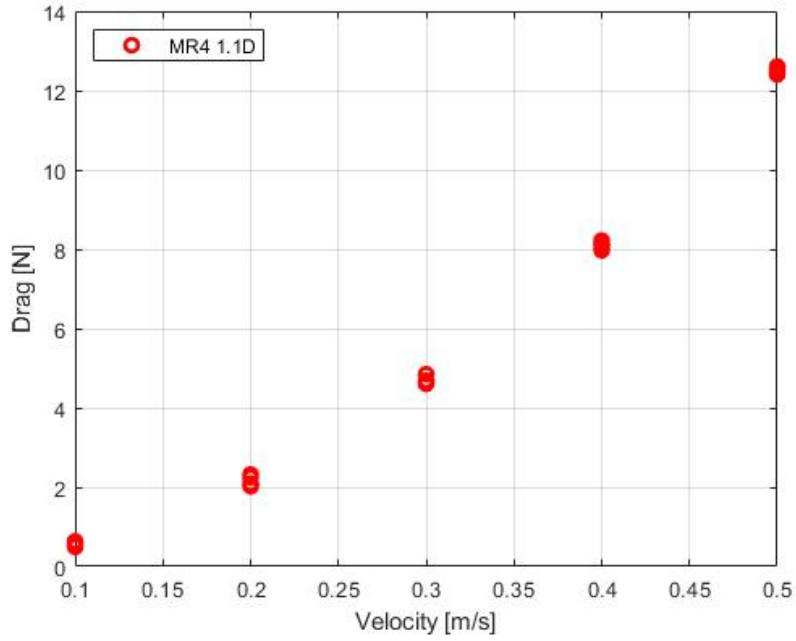
Figure 4-5: Results for MR4 drag vs velocity

4.2.5 **Results MR4 drag coefficient vs Reynolds number**

Figure 4-6 shows the drag coefficient for the MR4 with the increasing Reynolds number. The C_d stabilizes around 0.8 after hitting a Re of 50 000. Also, for the drag coefficient the same trend as for the MR7 can be seen, with a varying C_d at lower Reynolds numbers.
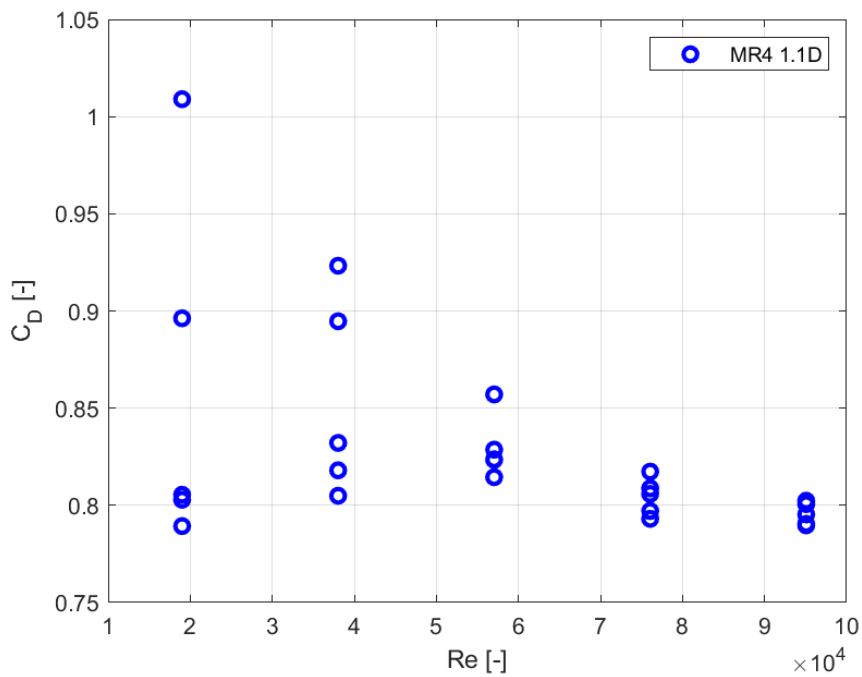
Figure 4-6: Results MR4 drag coefficient vs Reynolds number

31

4.2.6 **Results singlerotor**

The results for the 20 cm and 60 cm singlerotors are shown in *Figure 4-7*. The growth follows the same trend as the other results. The 60 cm disc have a clearly higher value of drag forces, due to the greater swept area. The graph shows 27 N and 4 N as the peak values for the two SD, with the SD 60 cm having the former.
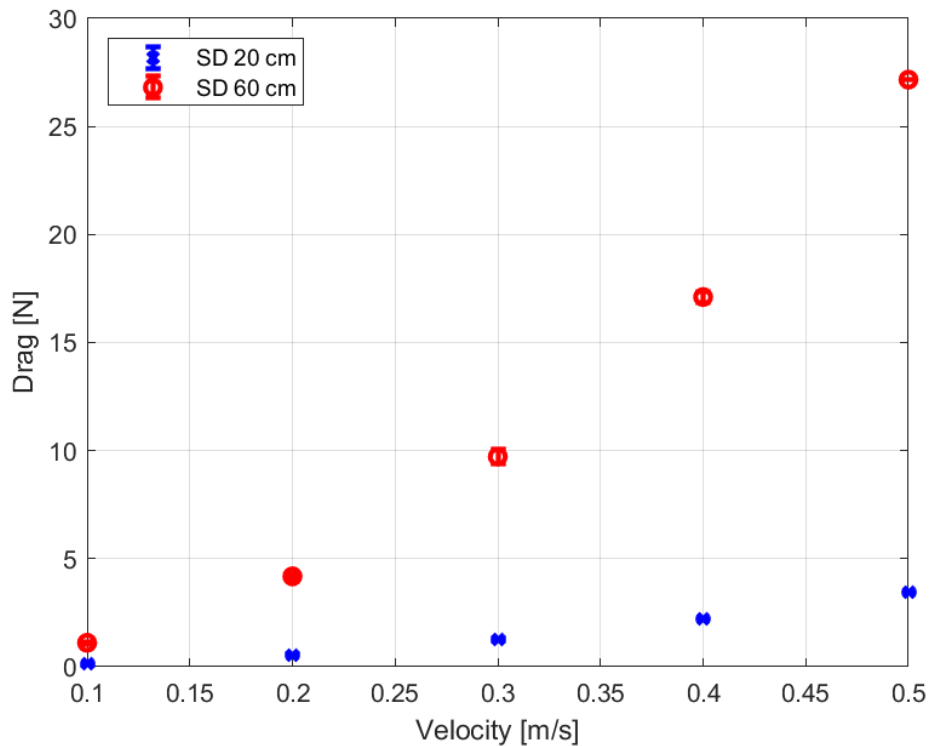
Figure 4-7: Results single disc drag vs velocity, SD 20 cm vs SD 60 cm

4.2.7 **Results singlerotor drag coefficient vs Reynolds number**

Figure 4-8 shows the results for the SD 20 cm and SD 60 cm. An interesting aspect is that the SD 20 cm has a higher drag coefficient than the SD 60 cm, which will be further discussed in chapter **5**. Both SD 20 cm and SD 60 cm have a stable C_d after 30 000 Re, respectively around 0.88 and 0.76. The SD 60 cm does not have the same difference C_d at lower Re, as seen in earlier trends. It should also be noted that the measurement for SD 60 cm at Re 96 000, only has one measurement, and this should be taken in consideration before used for comparing reasons.

Given the earlier trends showing stabilizing coefficients with increasing Re, and stable measurements of the C_d before Re at 96 000, it was still used in the graph.
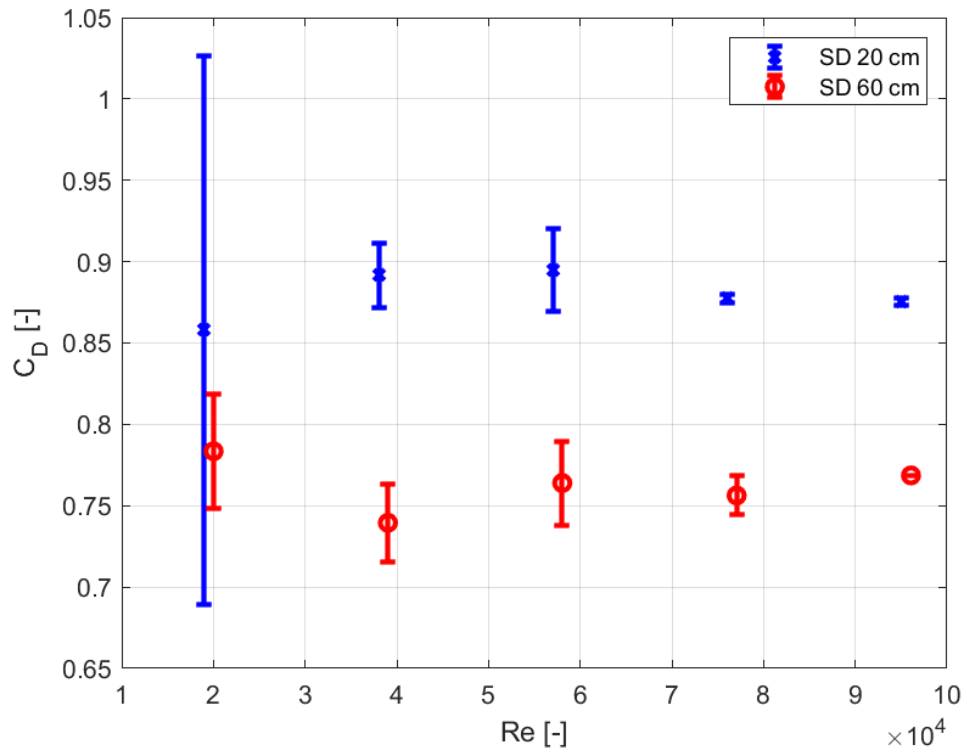
Figure 4-8: Results single disc drag coefficient vs Reynolds number

4.3 Comparison

4.3.1 MR7 theoretical and experimental results

Comparing the theoretical and the experimental results, there is a trend that the force value from the theoretical approach is slightly lower than the values from the experiment. The reason why the results are lower can be because of different neglected factors in the calculations. Even though the values are different, there is a mutual trend to be seen for both the approaches, with the force increasing quadratically. From the theoretical point of view the greatest increase is between 1.1D and 1.4D, which is expected because of the increase in materials from the support structure. In the experimental approach there are phenomenon's that will impact the outcome, for example the blockage effect, friction, and flow phenomenon. These impacts give the experimental results a slightly larger rise between 1.0D and 1.1D, which differs from the theoretical approach. The drag coefficient from the theoretical is a flat line, with no increase or decrease with increasing Re. The experimental results show an overall higher C_d, that varies a bit, and stabilizes with increasing Re. As shown in *Figure 4-9*.
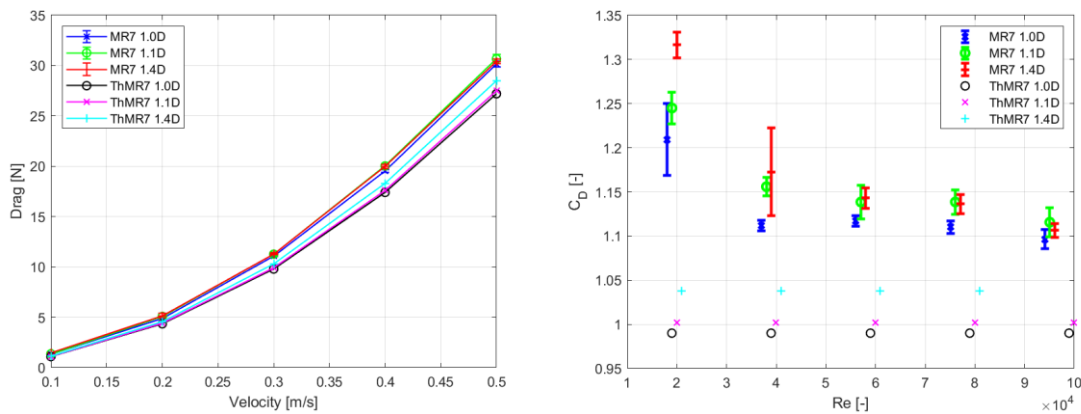
Figure 4-9: Theoretical and experimental comparison for drag force and drag coefficient for MR7

4.3.2 MR4 theoretical and experimental results

Comparing theoretical and experimental results for the force of the MR4 show similarities to MR7 with overall lower values for all the experimental results. The drag coefficient shows a greater difference with the experimental results stabilizing at a C_d of 0.8, giving a coefficient about 0.2 lower than the theoretical.
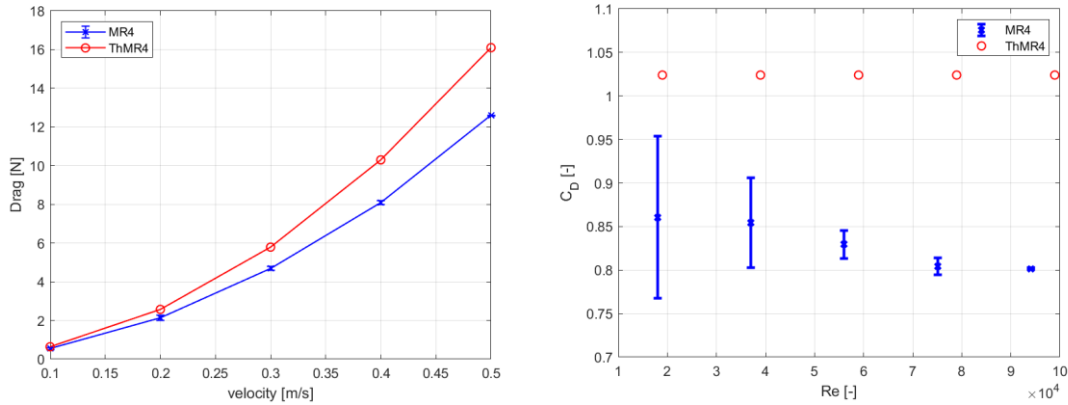
Figure 4-10: Theoretical and experimental comparison for drag force and drag coefficient for MR4

4.3.3 **MR7 vs MR4**

Comparing MR4 with MR7 shows overall lower drag forces for MR4, which is to be expected, given the measurements show a total drag force for the whole area of the system. An increase in area from the seven discs, provides a greater drag force. *Figure 4-11*: Results MR comparison, drag vs velocity clearly shows the relation between drag and velocity is applicable for all the MR-systems, with a doubling of velocity giving four times the force.
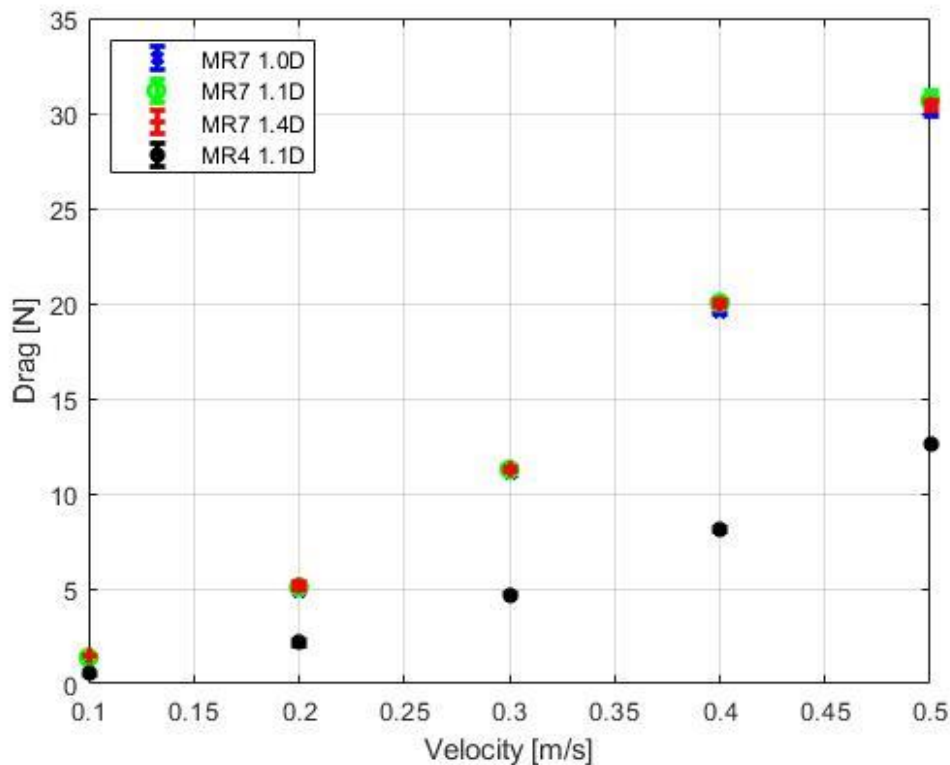
Figure 4-11: Results MR comparison, drag vs velocity

Figure 4-12 shows the comparison in drag coefficient. The differences in drag coefficient between the MR4 and MR7 raises a few questions as the differences were not expected to be as large. The drag coefficient formula is similar for the two in terms of fluid density and velocity, giving the relation between the drag force and area as the only variables between them. A possible explanation for this could be the blockage effect, which will be explained further in chapter **5**. It is interesting to see that the differences are this noticeable, even though there can be no explanation without further research on the subject.
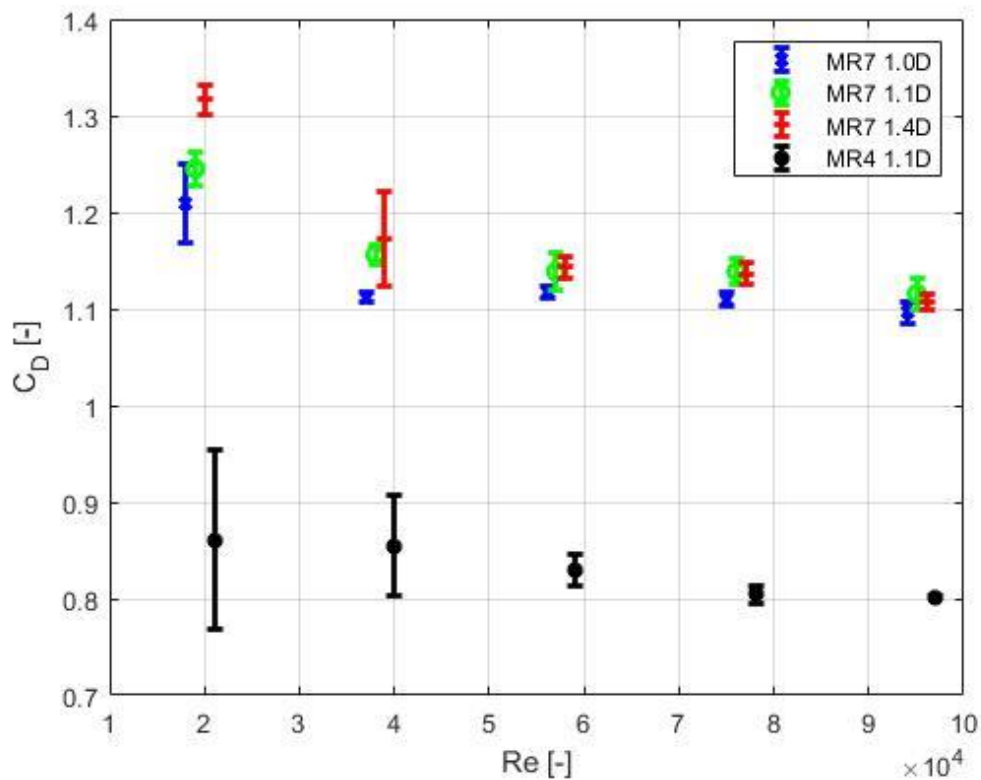
Figure 4-12: Results MR comparison, drag coefficient vs Reynolds number

5. Discussion

The interesting thing when looking at the drag with the different distances between the discs, raising the question, is there an optimum distance? This is what Nishino and Willden investigated in the report consisting of tidal turbines, where they looked at the relation between blockage and distance between turbines [14]. What they experienced by surveying the effect of underwater turbines was an optimum distance which gave the greatest power output. The question is, can the experiment and results for this project confirm what they discovered in the report from tidal turbines? From the results it looks like a difference that can lead to an optimum. Since the optimum turbine distance that Nishino and Willden found was 1.25 diameter, there will be an assumption that the drag will start to decrease a place before the distance reaches 1.4 diameter, but an exact optimum distance was difficult to find in this experiment. If the tests were set with multiple distances between 1.1D and 1.4D it might be possible to observe an optimum in this area. The differences are so small that it is hard to conclude after only this experiment, but it indicates that Nishino and Willden have a valid point.

Blockage effect is a known phenomenon in tidal energy, but not as applicable for singlerotor wind turbines. This is because the wind turbine usually has a larger distance between each turbine, inter turbine spacing, and there will not be more turbines in the vertical direction. In tidal energy they draw advantage from this, so can the same be done with the MR? From this experiment alone, it is complicated to conclude anything, but as mentioned there are indications of an optimal distance between the discs. Looking at a MR7 the center rotor will be the most affected by the blockage. As stated in the comparing results between MR4 and MR7, a possible explanation for the great difference in C_d values, could be caused by the blockage effect. The middle disc is affected by the surrounding discs, causing an uneven load force, with the maximum force applied to the center disc. If the same theory is set for the MR4, the maximum force would be in the gap between the four discs in the middle, causing a lower force measured on the MR4 system. On the other hand, one could argue that increasing the gap between the discs in the MR7 system could create similar force 'sinks', even though the comparing results for MR7 shows no indication of this. Even though blockage effect is, as mentioned, a known phenomenon, it needs more research to be able to understand it and conclude with questions like the ones above. Potential next step could be to research the drag forces on all the separate rotors of a MR setup and look at the differences.

Scaling is important when developing new technology within wind energy, but there is also a question if this is accurate enough and will show the right results in full scale. There should be taken precautions when using geometrical scaling. A small-scale experiment takes place in steady conditions but in full scale the turbine will be exposed to more uncontrollable variables. These

variables are not always easy to predict and should not occur in controlled environments. There may also appear other variables in the small-scale experiment that makes the result unsure.

For the multirotor some of the support structure is set behind disc, and sets a question of how much the disc influences the drag forces on the support structure. It can be debated of how much of the area of the structure should be included during the calculation considering that most of the structures will be behind the disc. For the theoretical part, separate drag forces were calculated for the support structure, and for the discs, and the full length of the support structure was used. Another potential step in MR research could be to research the impact the discs or rotors have on the structure behind it, giving an empiric database, making it easier to calculate for the future.

6. Conclusion

To summarise this experiment there are several things that have been discovered, most of them expected, but some unexpected. Given the research and experiment conducted in this thesis there is an indication that there may be an optimum distance between 1.1D and 1.4D. This matches with what Nishino and Willden discovered when they found an optimum distance of 1.25D. The reason why may be due to the blockage effect that occurs in the MR-system. The comparison between the experimental and theoretical result, the drag coefficient is more stable for the theoretical calculations, where the experimental result shows higher values for low Reynolds numbers. On the other hand, the drag forces tend to be more equal for the two approaches with a square growth.

To conclude it is a complex question if multirotors are more cost efficient than the singlerotors. The question takes in factors that makes it impossible to be answered after ''just'' a thesis comparing theoretical and experimental results. On the other hand, these results show that there are some interactions between the single rotor discs in a multirotor setup. These interactions are not captured by simple additive drag calculations and need further research and empirical results to compensate the lack of variables. The results do provide useful data for further research, which is an important input for detailed computational simulations on MR setups and can serve as a base for future cost-effective designs.

7. References

[1] UNFCCC, "United Nations Framework Convention on Climate Change," United Nations Framework Convention on Climate Change, [Online]. Available: https://unfccc.int/process-and-meetings/the-paris-agreement/the-paris-agreement. [Accessed 22 April 2021].

[2] BP, "Statistical Review of World Energy," BP, London, 2020.

[3] Equinor, "equinor.com," equinor, 2018. [Online]. Available: https://www.equinor.com/no/what-we-do/solar.html. [Accessed 20 April 2021].

[4] International Renewable Energy Agency, "IRENA," 2019. [Online]. Available: https://www.irena.org/wind. [Accessed 22 mars 2021].

[5] G. Prakash and H. Anuta, "FUTURE OF WIND," IRENA - International Renewable Energy Agency, 2019.

[6] GE Renewable Energy, "GE Renewable Energy," GE Renewable Energy, [Online]. Available: https://www.ge.com/renewableenergy/wind-energy/offshore-wind/haliade-x-offshore-turbine. [Accessed 22 Mars 2021].

[7] Vestas, "vestas.com," vestas, 2021. [Online]. Available: https://www.vestas.com/en/products/offshore-platforms/v236_15_mw#!technical-specifications. [Accessed 25 april 2021].

[8] Siemens Gamesa, "Siemens Gamesa Renewable Energy," Siemens , [Online]. Available: https://www.siemensgamesa.com/products-and-services/offshore/wind-turbine-sg-14-222-dd. [Accessed 27 April 2021].

[9] E. Topham and D. McMillan, "Sustainable decommissioning of an offshore wind farm," University of Strathclyde, Glasgow, 2016.

[10] D. McMillan and I. Dinwoodie, "Forecasting Long Term Jack up Vessel Demand for Offshore Wind," University of Strathclyde, Department of Electronics and Electrical Engineering, Glasgow, 2012.

[11] C. Martin, "Bloomberg green," Bloomberg green, 5 Februar 2020. [Online]. Available: https://www.bloomberg.com/news/features/2020-02-05/wind-turbine-blades-can-t-be-recycled-so-they-re-piling-up-in-landfills. [Accessed 30 April 2021].

[12] J. Bartl, F. Pierella and L. Sætran, "Wake measurements behind an array of two," Norwegian University of Science and Technolog, Trondheim, 2012.

[13] J. Sørensen, "Numerical Actuator Disk Models," in *Wind energy*, 2012.

[14] T. Nishino and R. Wilden, "The efficiency of an array of tidal turbinespartially blocking a wide channel," J. Fluid Mech, London, 2012.

[15] L. B. &. S. Matysik, "Wind turbine models," 28 august 2016. [Online]. Available: https://en.wind-turbine-models.com/turbines/1459-vestas-multi-rotor-concept. [Accessed 22 april 2021].

[16] M. A. Majid Bastankhah, "www.Sciencedaily.com," Aarhus University, 16 October 2019. [Online]. Available: www.sciencedaily.com/releases/2019/10/191016124541.htm. [Accessed 22 April 2021].

[17] J. Barlow, W. Rae. Jr and A. Pope, Low-speed Wind Tunnel Testing, New York: John Wiley & Sons, 1999.

[18] B. Karlsen and L. R. Sætran, "Cross-sectional wake measurements of actuator disks," NTNU, Tronheim, 2019.

[19] S. Störtenbecker, M. Tamang and P. Dalhoff, "Simplified support structure design for multi rotor wind turbine systems," in *Wind EnergyScience Conference*, Cork, 2019.

[20] M. A. Mendez, M. Di Nardo and C. Benocci, "www.Researchgate.net," March 2017. [Online]. Available: https://www.researchgate.net/figure/Variation-of-cylinder-drag-coefficient-with-Reynolds-number-Source-Experimental-data_fig22_316588041. [Accessed 21 May 2021].

[21] H. Schlichting, "Thermopedia," McGraw-Hill Inc, 16 march 2011. [Online]. Available: https://www.thermopedia.com/content/637/. [Accessed 22 march 2021].

List of figures

List of tables

Attachments

Attachment 1: Theoretical approach in Excel

Attachment 2: Model joints CAD drawings

Attachment 3: Experimental results in MatLab